

# Supplementary Information for

## Thermogenic hydrocarbon biodegradation by diverse depth-stratified microbial populations at a Scotian Basin cold seep

Xiyang Dong<sup>1, 2, \*</sup>, Jayne E. Rattray<sup>2</sup>, D. Calvin Campbell<sup>3</sup>, Jamie Webb<sup>4</sup>, Anirban Chakraborty<sup>2</sup>, Oyeboade Adebayo<sup>2</sup>, Stuart Matthews<sup>2</sup>, Carmen Li<sup>2</sup>, Martin Fowler<sup>4</sup>, Natasha M. Morrison<sup>5</sup>, Adam Macdonald<sup>5</sup>, Ryan A. Groves<sup>2</sup>, Ian A. Lewis<sup>2</sup>, Scott H. Wang<sup>2</sup>, Daisuke Mayumi<sup>6</sup>, Chris Greening<sup>7, 8</sup>, Casey R.J. Hubert<sup>2, \*</sup>

<sup>1</sup> School of Marine Sciences, Sun Yat-Sen University, Zhuhai, 519082, China

<sup>2</sup> Department of Biological Sciences, University of Calgary, Calgary, AB T2N 1N4, Canada

<sup>3</sup> Geological Survey of Canada-Atlantic, Dartmouth, NS B3B 1A6, Canada

<sup>4</sup> Applied Petroleum Technology (Canada), Calgary, AB T2N 1Z6, Canada

<sup>5</sup> Nova Scotia Department of Energy and Mines, Halifax, NS B2Y 4A2, Canada

<sup>6</sup> Institute for Geo-Resources and Environment, Geological Survey of Japan, National Institute of Advanced Industrial Science and Technology (AIST), 1-1-1 Higashi, Tsukuba, 305-8567, Japan

<sup>7</sup> School of Biological Sciences, Monash University, Clayton, VIC 3800, Australia

<sup>8</sup> Department of Microbiology, Biomedicine Discovery Institute, Monash University, Clayton, VIC 3800, Australia

\* Corresponding authors.

Emails: dongxy23@mail.sysu.edu.cn (X.D.); chubert@ucalgary.ca (C.R.J.H.)

## Supplementary Note 1

To understand the wider metabolic capabilities of these cold seep microbial communities, metabolomic analysis was combined with gene-centric analysis of quality-filtered reads, as well as genome-centric analysis of the 376 MAGs.

With respect to organotrophy, genes for the degradation of complex carbohydrates and peptides were prevalent. In total, ~7454 potential carbohydrate-active enzymes (CAZymes) were detected, most notably glycoside hydrolases, carbohydrate esterases, and polysaccharide lyases<sup>1</sup>; CAZymes were numerous in bacterial lineages such as Planctomycetes, Bacteroidetes, and Armatimonadetes (**Supplementary Data 6**). Annotated peptidases were more evenly distributed across bacteria and archaea, with the highest proportions found in genomes assigned to Patescibacteria, *Dehalococcoidia*, Aerophobetes, and Atribacteria (**Figure 3a and Supplementary Data 7**). Consistent with these genomic observations, metabolites associated with carbohydrate and peptide hydrolysis were detected (e.g. glucose and sucrose) (**Figure 3b**). Many community members also possess gene sets to convert hydrolysis products to pyruvate through the Embden-Meyerhof-Parnas (185 MAGs) and Entner-Doudoroff (51 MAGs) pathways (**Figure 3b and Supplementary Data 5**). Accordingly, both glucose 6-phosphate and pyruvate were detected in the sediment metabolomes (**Figure 3b**). Most genomes also encoded the potential to ferment pyruvate to formate (119 MAGs), acetate (270 MAGs), lactate (14 MAGs), and ethanol (94 MAGs), as well as the potential for hydrogen production via abundant [FeFe]-hydrogenases associated with fermentation or group 3 [NiFe]-hydrogenases<sup>2</sup> (**Figure 3a, Supplementary Figure 11 and Supplementary Data 5**). The ability to degrade fatty acids and other organic acids via beta-oxidation was common to Lokiarchaeota, Chloroflexi, and Proteobacteria (**Supplementary Data 8**), with associated metabolites also detected (e.g. 6-carboxyhexanoate, 10-hydroxydecanoate, and other carboxylic acids) (**Figure 3b**).

The most prevalent carbon fixation pathways in these sediments are the Calvin-Benson cycle (68 MAGs), Wood-Ljungdahl pathway (114 MAGs), and 4-hydroxybutyrate cycle (4 MAGs) (**Figure 3a and Supplementary Data 5**), consistent with the abundance of

corresponding key metabolic genes (**Supplementary Figure 14**). The sediment microbial communities include various putative sulfide, thiosulfate, ammonia, nitrite, carbon monoxide, and hydrogen oxidizers (**Supplementary Data 5**), with provision of these compounds potentially via biological or geological processes. Canonical genes for sulfide oxidation (sulfide:quinone oxidoreductase and flavocytochrome *c* sulfide dehydrogenase) were found in 38 MAGs from diverse lineages (e.g. Proteobacteria, *Anaerolineales*, and Heimdallarchaeota) (**Supplementary Figures 3-4**). The oxidative bacterial-type DsrAB-type dissimilatory sulfite reductases<sup>3</sup> were detected in four genomes from *Alpha*- and *Gammaproteobacteria* potentially responsible for sulfide oxidation (**Supplementary Figure 5**). Five MAGs from *Epsilon*- and *Gammaproteobacteria* encoded genes for the SoxB component of the periplasmic thiosulfate-oxidizing Sox enzyme complex (**Supplementary Figure 6**). Genes for ammonia oxidation to hydroxylamine (ammonia monooxygenase) were detected in four Thaumarchaeota genomes (**Supplementary Figure 7**), while those associated with further oxidation of nitrite (nitrite oxidoreductase) were tentatively found in five MAGs affiliated to *Anaerolineales*, Acidobacteria, Actinobacteria, and Planctomycetes (**Supplementary Figure 8**). Gene abundance profiles suggest that these nitrogen metabolisms mainly occur in 0-20 cmbsf surface sediments (**Supplementary Figure 14**). Three MAGs belonging to Actinobacteria, Actinobacteria, and *Alphaproteobacteria* encoded carbon monoxide dehydrogenase large subunit (CoxL), a marker for carbon monoxide oxidation (**Supplementary Figure 9**). Ten phyla (58 MAGs) encoded group 1 and group 2 [NiFe]-hydrogenases associated with hydrogenotrophic respiration, with certain lineages, including *Deltaproteobacteria*, Planctomycetes, *Dehalococcoidia*, Actinobacteria, and Aerophobetes, encoding subgroups (1a, 1b) that support hydrogenotrophic sulfate reduction and halorespiration<sup>4, 5</sup> (**Supplementary Figure 10**). Additionally, 197 MAGs from 35 phyla encode cofactor-coupled group 3 [NiFe]-hydrogenases (**Supplementary Figure 11**) and energy-converting group 4 [NiFe]-hydrogenases (**Supplementary Figure 12**), both of which are known to be physiologically reversible<sup>2</sup>.

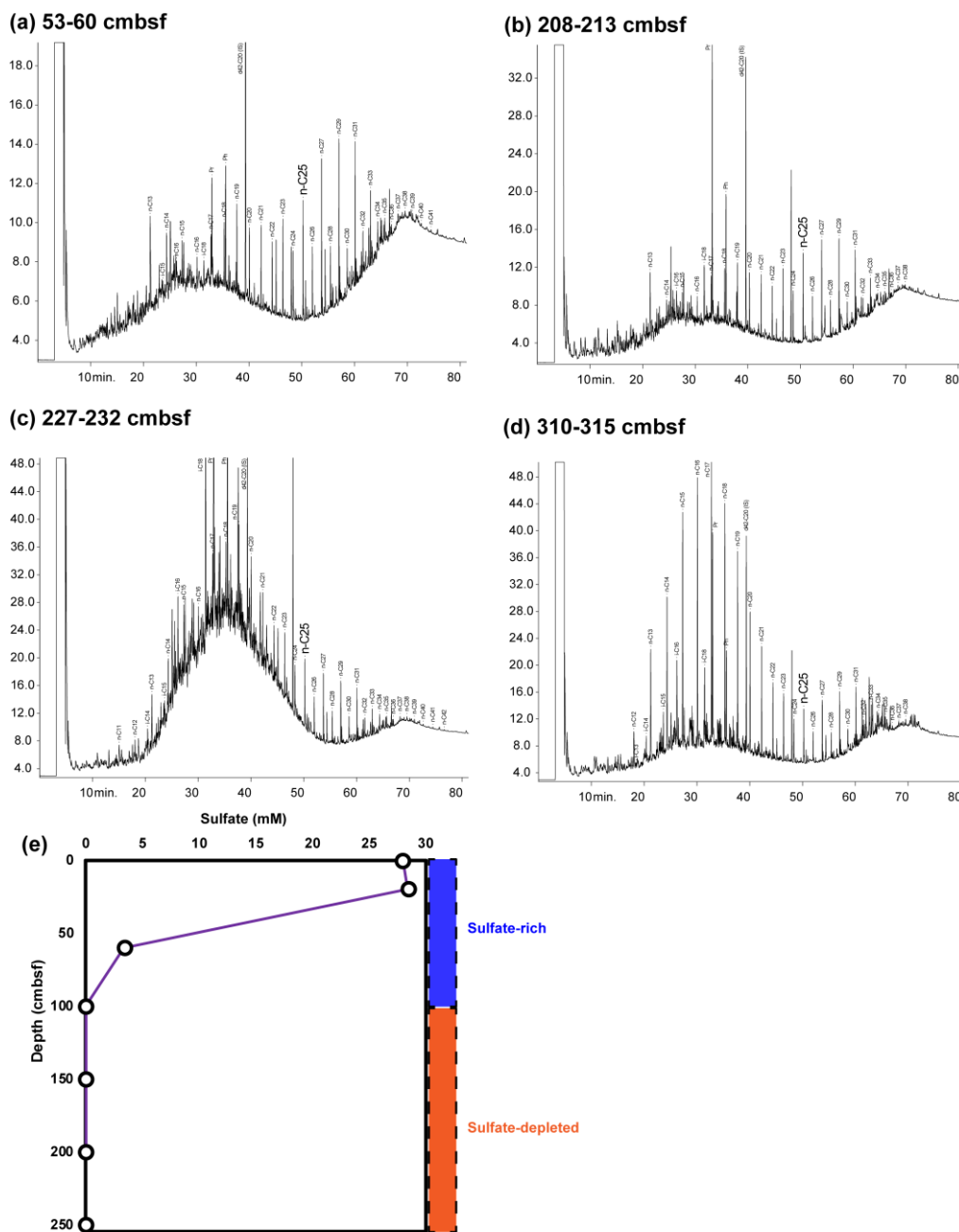
Metabolomics revealed organohalides as potential respiratory electron acceptors in the sediments, e.g. dichlorotoluene and dichlorodiphenyldichloroethane (**Figure 3b**).

Accordingly, reductive dehalogenases were encoded in 54 MAGs from 13 phyla, including lineages such as Chloroflexi, Lokiarchaeota, Bathyarchaeota, and Proteobacteria **(Supplementary Figure 13)**. Organisms encoding these enzymes may conserve energy by coupling oxidation of H<sub>2</sub> and other electron donors to the reduction of organochloride compounds like the ones detected in the sediments. Full gene sets for dissimilatory reduction of sulfate to sulfide (*sat*, *aprAB* and *dsrAB*) were found in 12 genomes from *Deltaproteobacteria* and *Zixibacteria* **(Supplementary Figure 5)**. Thirty bacterial members of these sediment communities are predicted to use nitrate or nitrite as electron acceptors, though none encoded all of the genes necessary for complete denitrification or dissimilatory nitrate reduction to ammonia **(Supplementary Data 5)**. Terminal oxidases were also detected, but in line with oxygen only permeating the upper centimeters of marine sediments, these genes were mainly found in lineages such as Proteobacteria and Thaumarchaeota that dominated the upper sediment layers **(Supplementary Figure 14)**.

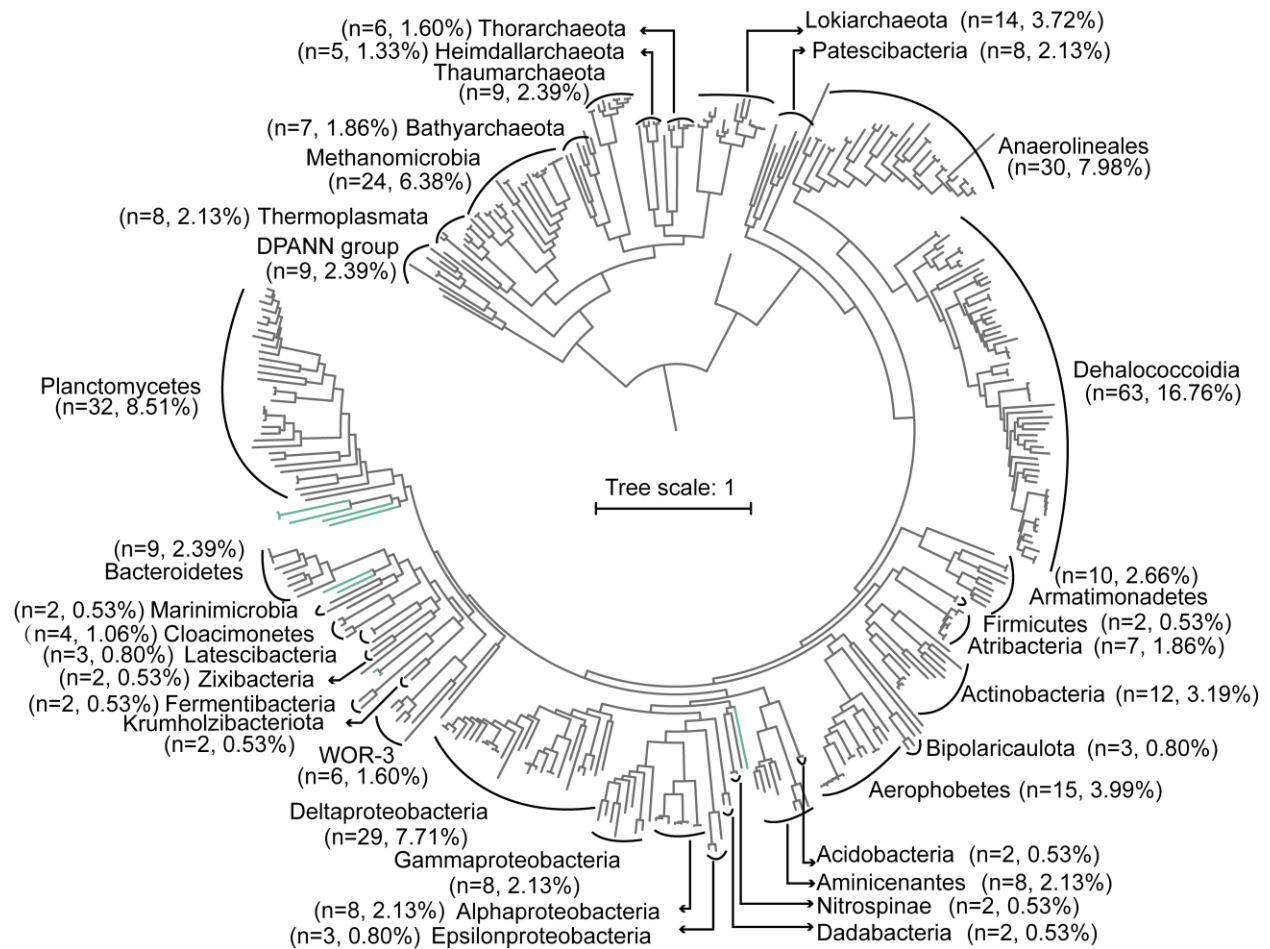
**Supplementary Table 1** Extractable organic matter compositions of four sediment subsamples.

Depth (cmbsf)		53-60	208-213	227-232	310-315
TOC (%)		0.25	0.35	0.36	0.56
EOM (mg/kg rock)		104	361	177	168
wt% of EOM	SAT	47.5	52.1	35.0	24.6
	ARO	10.0	11.8	13.9	12.5
	POL	42.5	26.5	17.9	36.4
	ASP	0.0	9.6	33.2	26.4
$\delta^{13}\text{C-Sat}$ (‰)		ND	-31.5	ND	ND
$\delta^{13}\text{C-Aro}$ (‰)		ND	-29.6	ND	ND

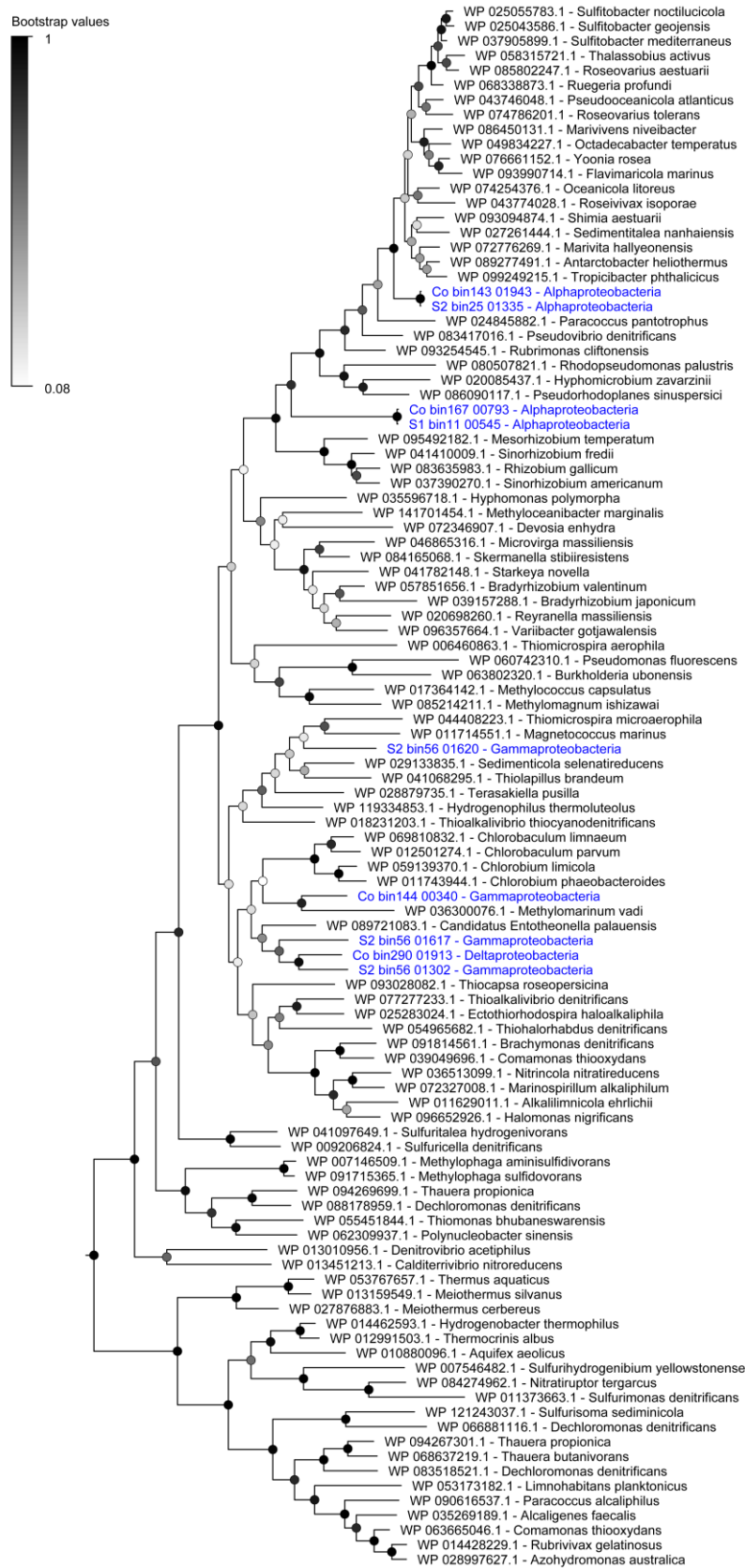
Abbreviations: TOC, total organic carbon; EOM, extractable organic matter; SAT, saturated hydrocarbons; ARO, aromatic hydrocarbons; POL, polars; ASP, asphaltenes; wt%, weight percentage; ND, not determined.



**Supplementary Figure 1** Extractable organic matter from subsampled sediments and sulfate concentrations from porewater. GC-FID chromatograms showing unresolved complex mixture (UCM) humps for four different depths including (a) 53-60 cmbsf, (b) 208-213 cmbsf, (c) 227-232 cmbsf, and (d) 310-315 cmbsf; (e) porewater concentrations of sulfate along depths. For (a)-(d), y-axis: detector response; x-axis: retention time (minutes). Additional parameters for the extractable organic matter of these samples are provided in **Supplementary Table 1**.

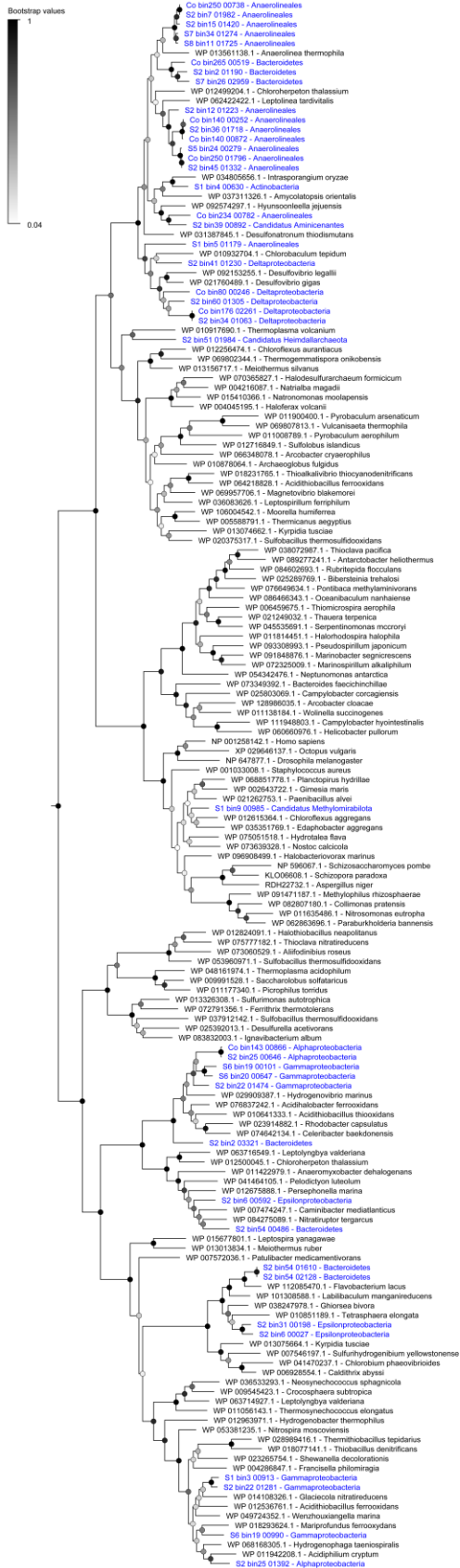


**Supplementary Figure 2** Phylogenetic placement of 376 reconstructed metagenome-assembled genomes. A maximum-likelihood phylogenomic tree was built based on concatenated amino acid sequences of 43 conserved single-copy genes using RAxML with the PROTGAMMALG model. The scale bar represents 1 amino acid substitution per sequence position. Numbers in parentheses show total MAGs recovered. Phyla with only one detected MAG are not labelled. Ten MAGs corresponded to unclassified phylum-level lineages (green branches; unlabelled). The full tree file with references is available in **Supplementary Data 4**.

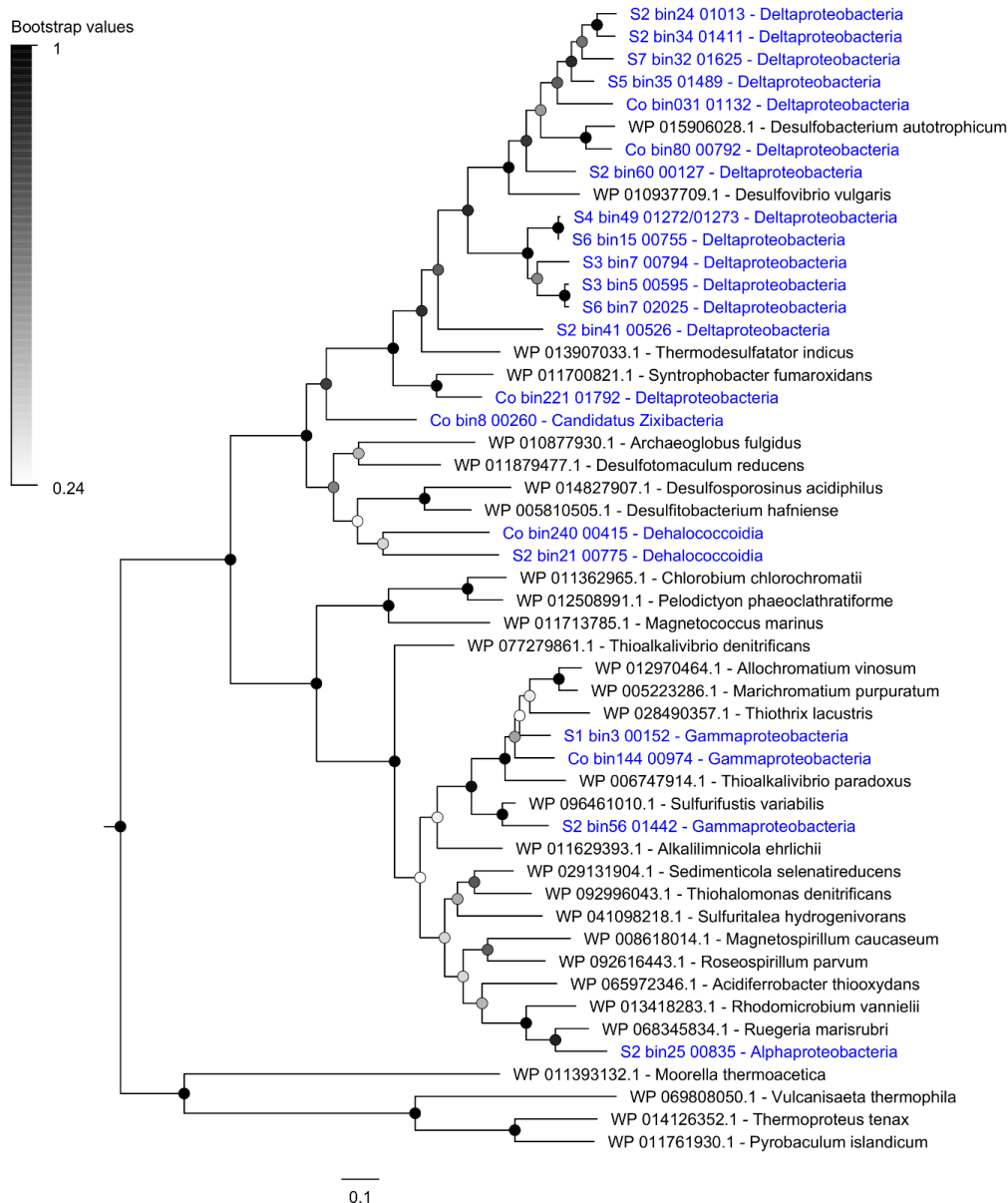




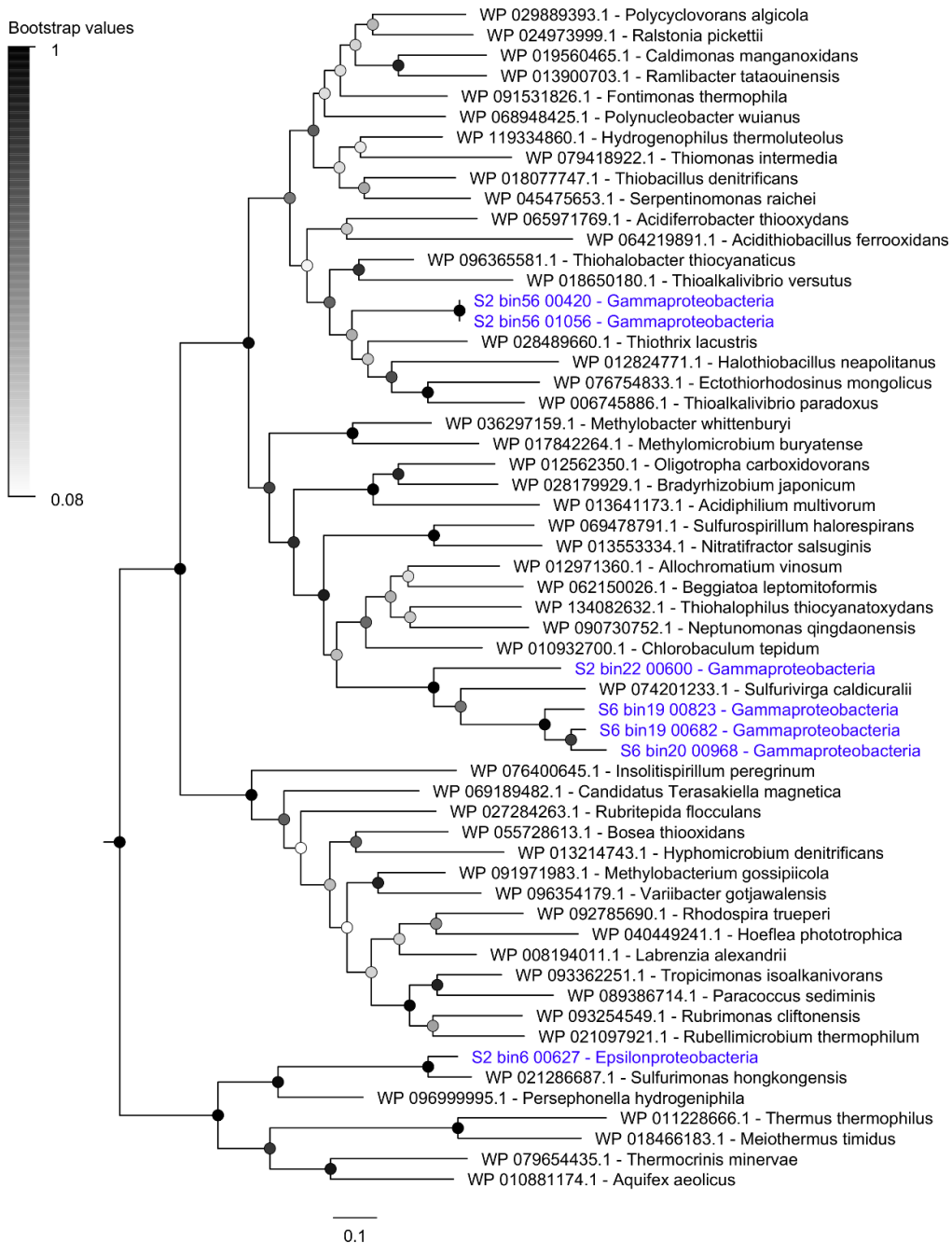
**Supplementary Figure 3** Maximum-likelihood tree of amino acid sequences of flavocytochrome *c* sulfide dehydrogenase (FCC), a marker for sulfide oxidation. The tree shows sequences from cold seep metagenome-assembled genomes obtained in this study (blue) alongside representative reference sequences (black). The tree was constructed using the JTT matrix-based model, used all sites, and was bootstrapped with 50 replicates and midpoint-rooted.



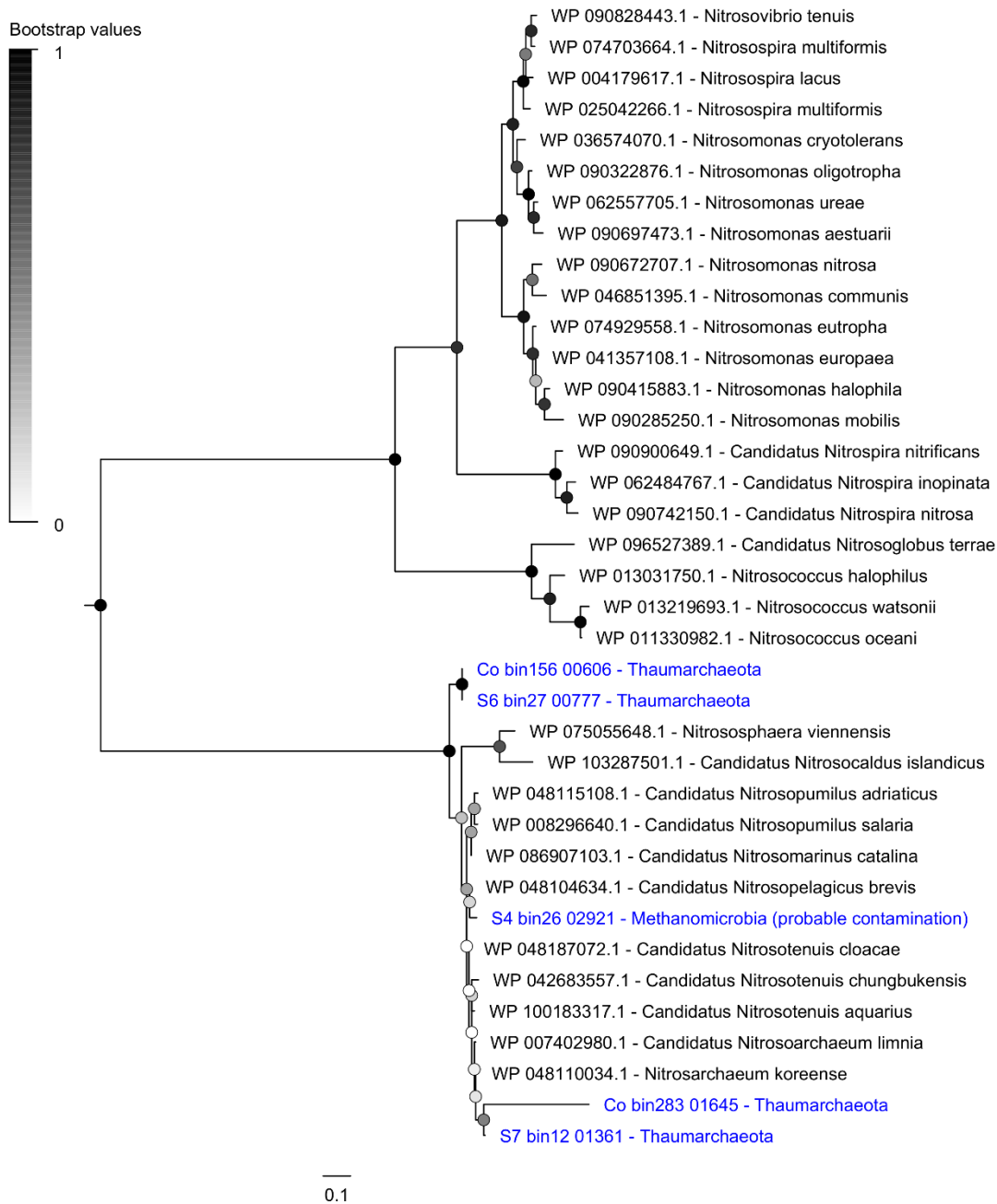
**Supplementary Figure 4** Maximum-likelihood tree of amino acid sequences of the sulfide-quinone oxidoreductase (Sqr), a marker for sulfide oxidation. The tree shows sequences from cold seep metagenome-assembled genomes obtained in this study (blue) alongside representative reference sequences (black). The subgroup of each reference sequence is denoted. The tree was constructed using the JTT matrix-based model, used all sites, and was bootstrapped with 50 replicates and midpoint-rooted.



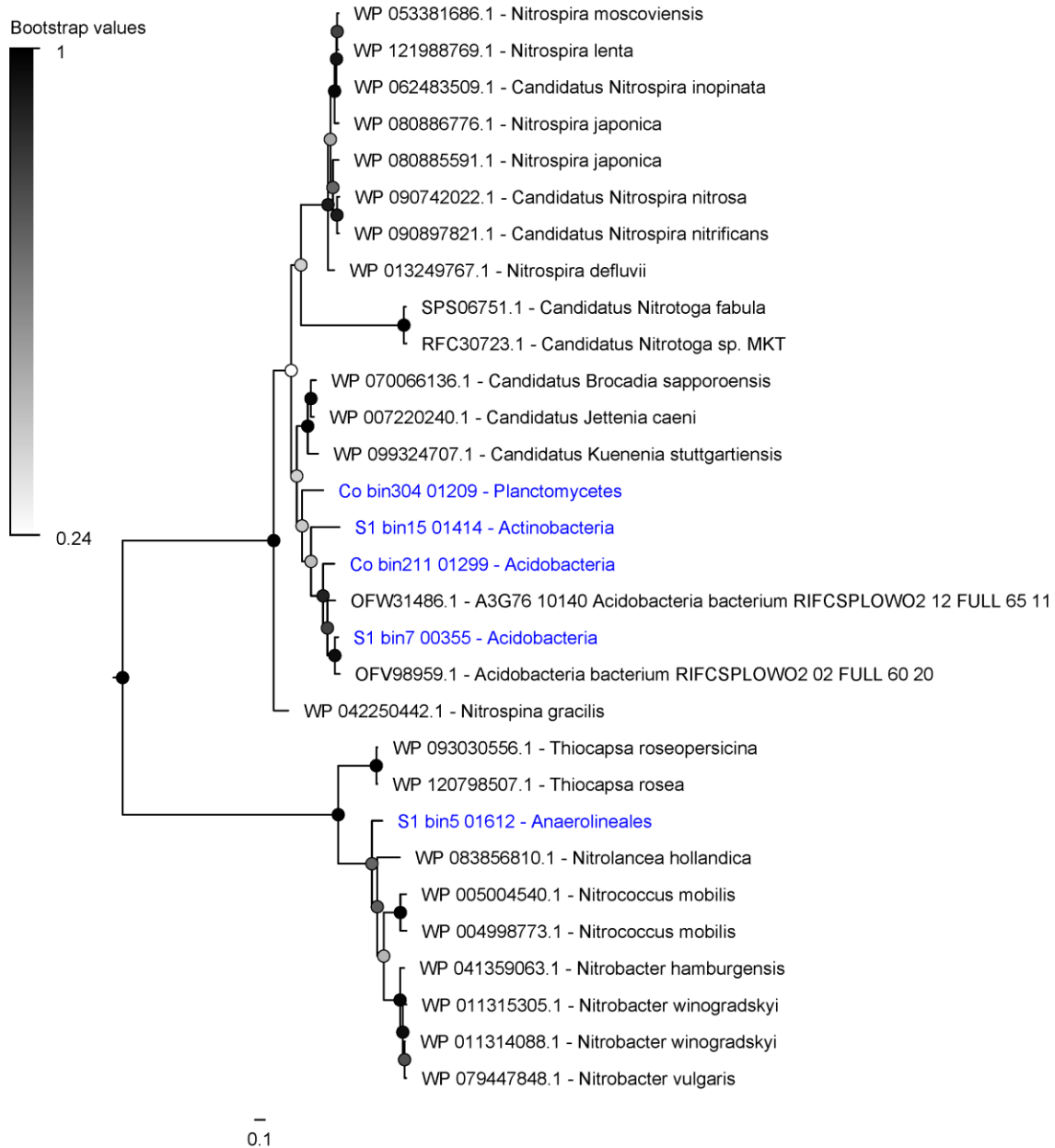
**Supplementary Figure 5** Maximum-likelihood tree of amino acid sequences of dissimilatory sulfite reductase A subunit (DsrA). The tree shows sequences from cold seep metagenome-assembled genomes obtained in this study (blue) alongside representative reference sequences (black). This enzyme is a marker for dissimilatory sulfite reduction (top and bottom major clades; *Deltaproteobacteria*, Zixibacteria, *Dehalococcoidia* bins) and sulfide oxidation (middle clade; *Gammaproteobacteria* and Alphaproteobacteria bins). The tree was constructed using the JTT matrix-based model, used all sites, and was bootstrapped with 50 replicates and midpoint-rooted.



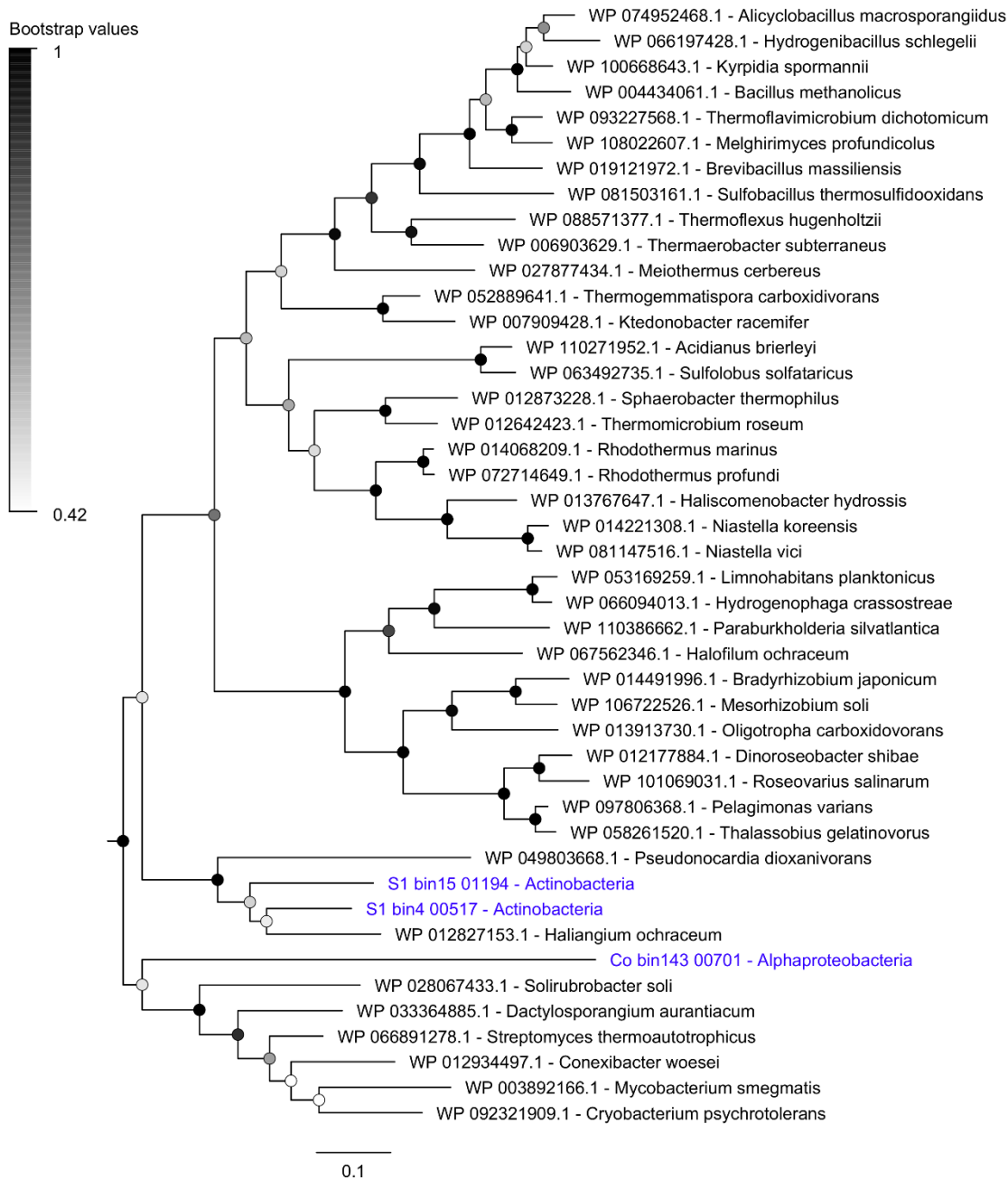
**Supplementary Figure 6** Maximum-likelihood tree of amino acid sequences of the thiosulfohydrolase (SoxB), a marker for thiosulfate oxidation. The tree shows sequences from cold seep metagenome-assembled genomes obtained in this study (blue) alongside representative reference sequences (black). The subgroup of each reference sequence is denoted. The tree was constructed using the JTT matrix-based model, used all sites, and was bootstrapped with 50 replicates and midpoint-rooted.



**Supplementary Figure 7** Maximum-likelihood tree of amino acid sequences of ammonia monooxygenase A subunit (AmoA), a marker for ammonia oxidation during aerobic nitrification. The tree shows sequences from cold seep metagenome-assembled genomes obtained in this study (blue) alongside representative reference sequences (black). The tree was constructed using the JTT matrix-based model, used all sites, and was bootstrapped with 50 replicates and midpoint-rooted.

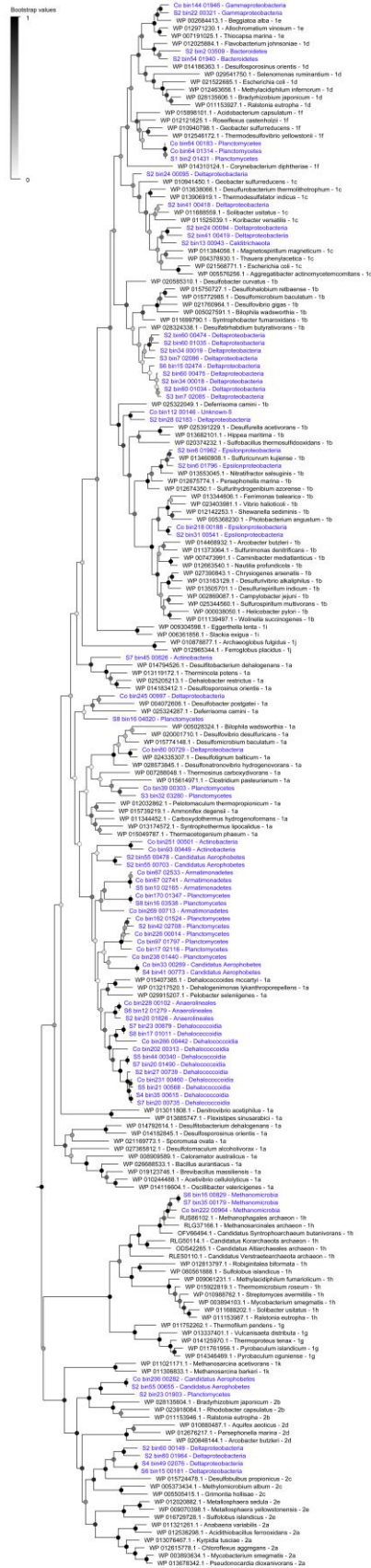


**Supplementary Figure 8** Maximum-likelihood tree of amino acid sequences of the nitrite oxidoreductase A subunit (NxrA), a marker for nitrite oxidation during aerobic nitrification. The tree shows sequences from cold seep metagenome-assembled genomes obtained in this study (blue) alongside representative reference sequences (black). The subgroup of each reference sequence is denoted. The tree was constructed using the JTT matrix-based model, used all sites, and was bootstrapped with 50 replicates and midpoint-rooted.

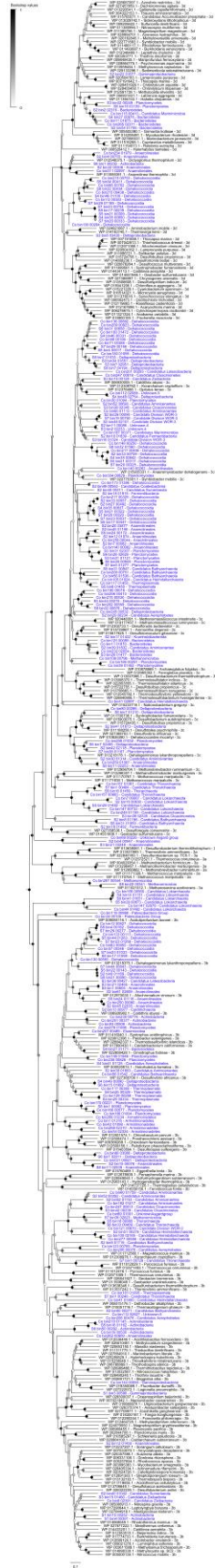


**Supplementary Figure 9** Maximum-likelihood tree of amino acid sequences of carbon monoxide dehydrogenase large subunit (CoxL), a marker for aerobic carbon monoxide oxidation. The tree shows sequences from cold seep metagenome-assembled genomes obtained in this study (blue) alongside representative reference sequences (black). The tree was constructed using the JTT matrix-based model, used all sites, and was bootstrapped with 50 replicates and midpoint-rooted.

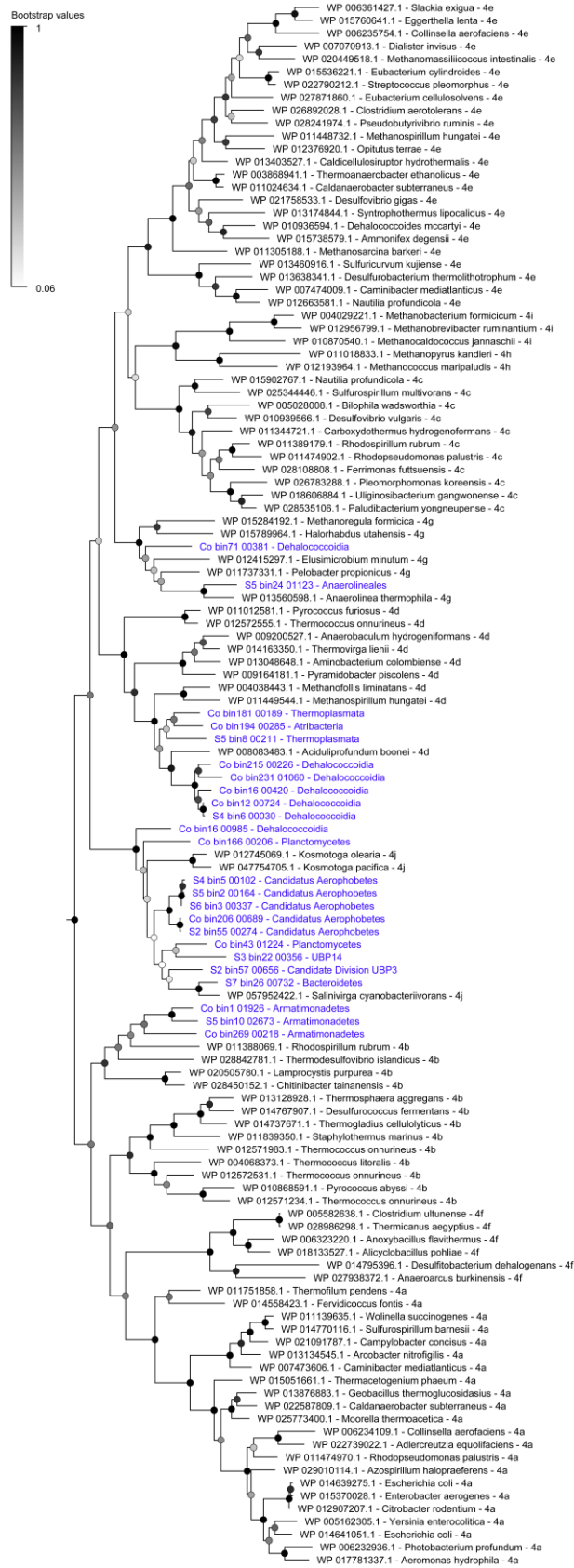




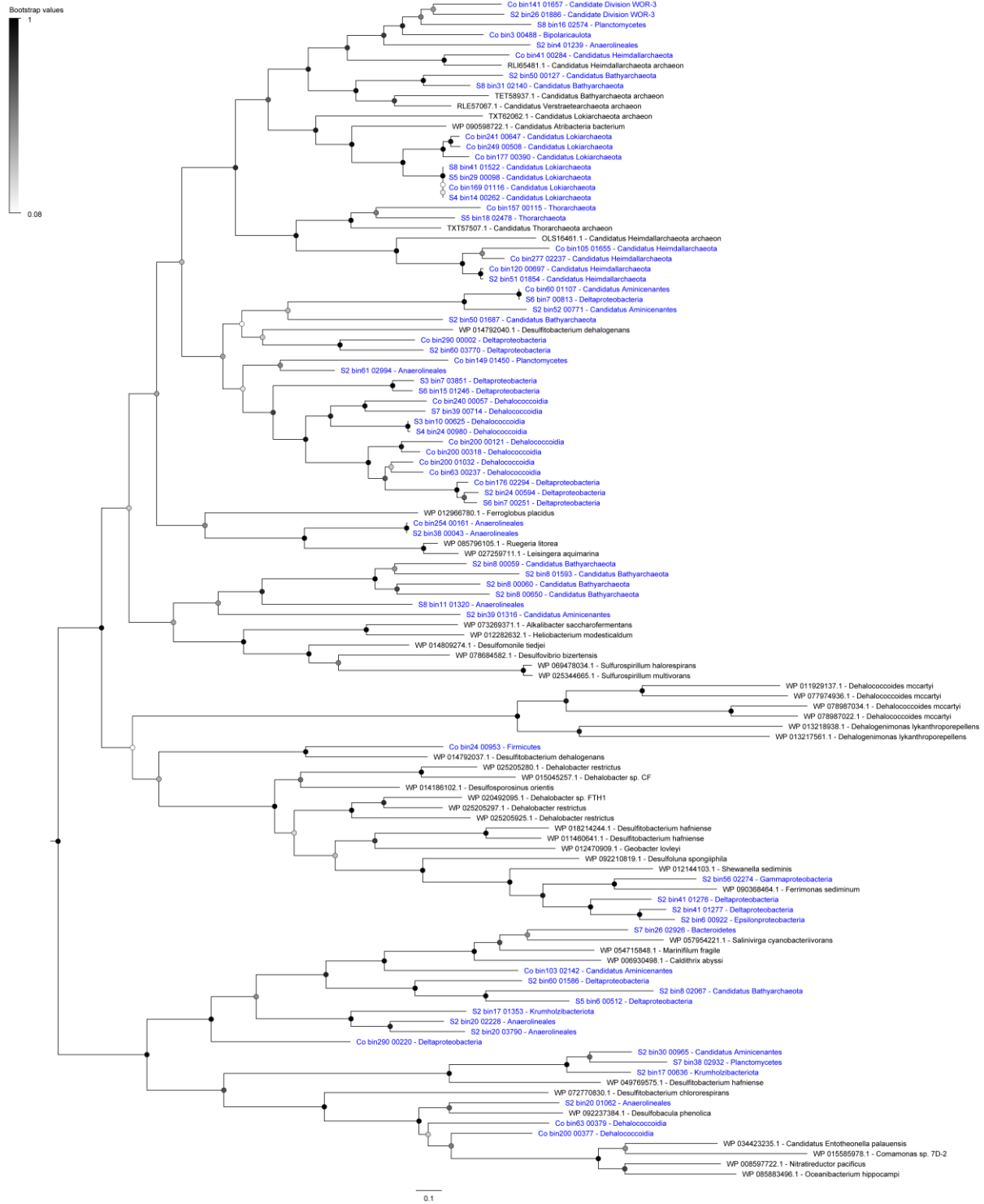
**Supplementary Figure 10** Maximum-likelihood tree of amino acid sequences of group 1 and 2 [NiFe]-hydrogenase large subunits, a marker for hydrogen oxidation during respiratory processes. The tree shows sequences from cold seep metagenome-assembled genomes obtained in this study (blue) alongside representative reference sequences (black). The subgroup of each reference sequence is denoted according to the HydDB classification scheme. The tree was constructed using the JTT matrix-based model, used all sites, and was bootstrapped with 50 replicates and midpoint-rooted.



**Supplementary Figure 11** Neighbour-joining tree of amino acid sequences of the group 3 [NiFe]-hydrogenase large subunit, a marker for bidirectional hydrogen metabolism during various processes. The tree shows sequences from cold seep metagenome-assembled genomes obtained in this study (blue) alongside representative reference sequences (black). The subgroup of each reference sequence is denoted according to the HydDB classification scheme. The tree was constructed using the Poisson model with gaps treated with pairwise deletion, was bootstrapped with 50 replicates, and was midpoint-rooted. To enable neighbour-joining, 54 incomplete sequences of the original 298 hits were excluded from this analysis.



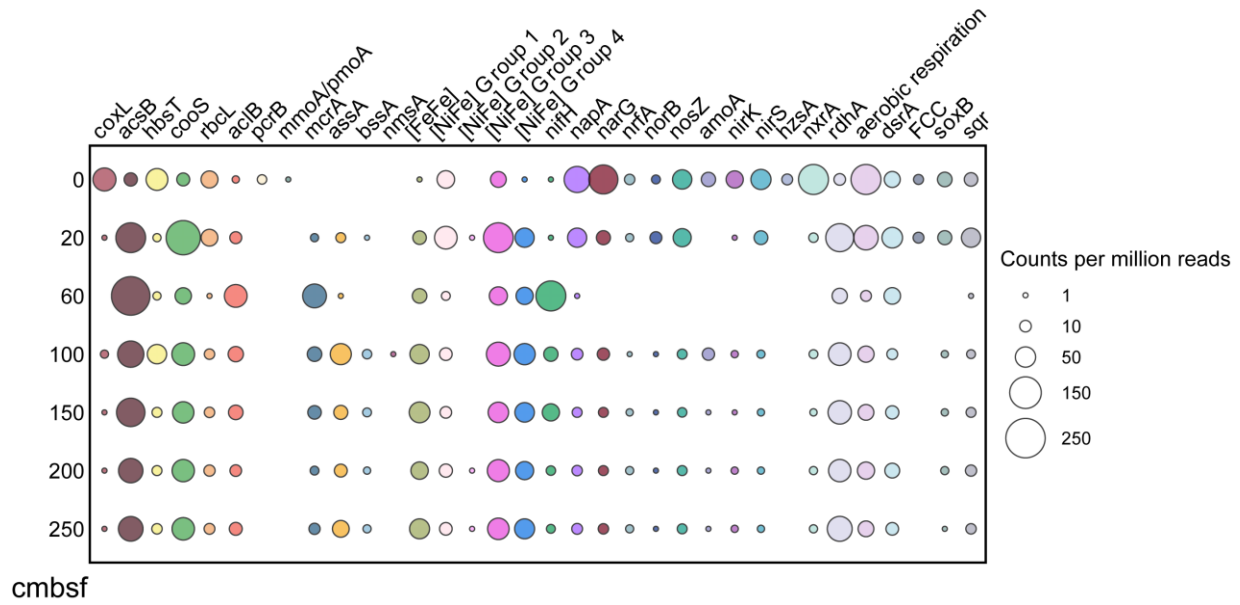
**Supplementary Figure 12** Maximum-likelihood tree of amino acid sequences of the group 4 [NiFe]-hydrogenase large subunit, a marker primarily for hydrogen production during fermentative and respiratory processes. The tree shows sequences from cold seep metagenome-assembled genomes obtained in this study (blue) alongside representative reference sequences (black). The subgroup of each reference sequence is denoted according to the HydDB classification scheme. The tree was constructed using the JTT matrix-based model, used all sites, and was bootstrapped with 50 replicates and midpoint-rooted.



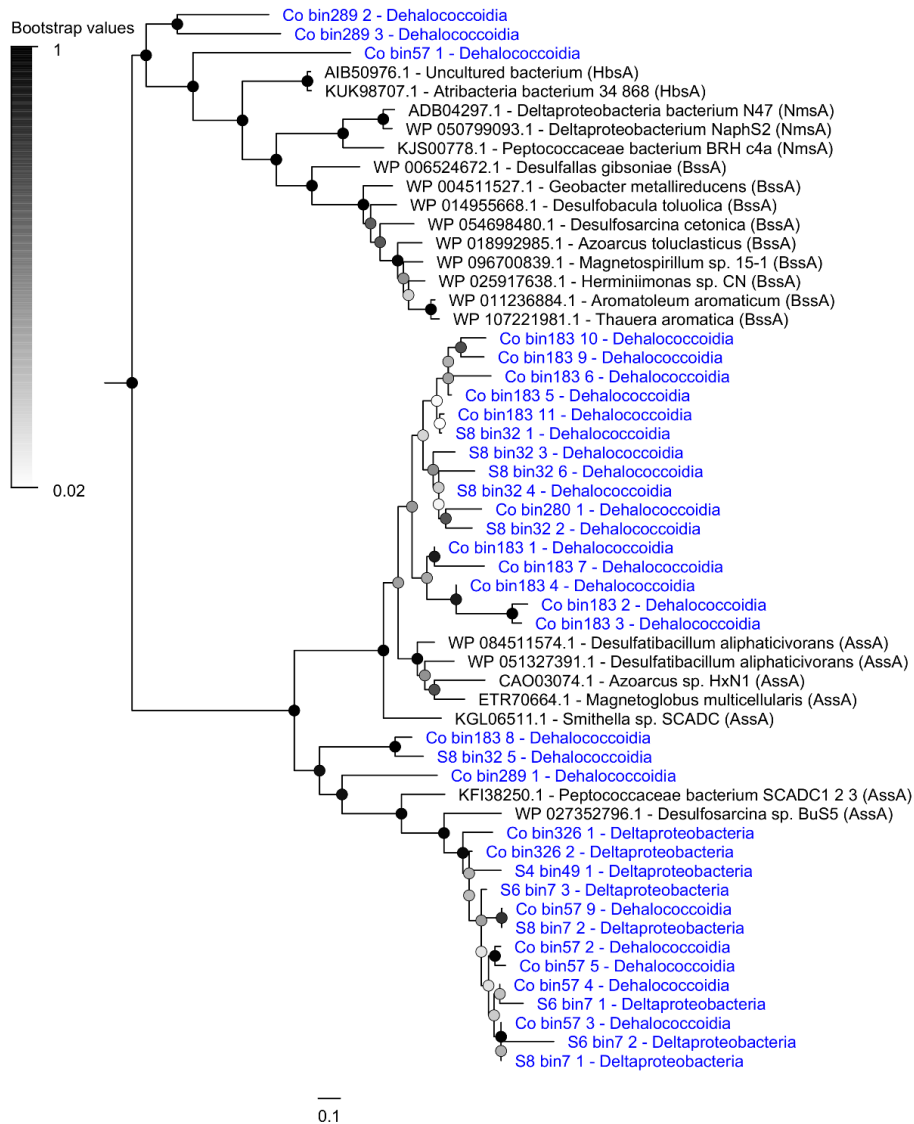
**Supplementary Figure 13** Maximum-likelihood tree of amino acid sequences of the reductive dehalogenase A subunit (RdhA), a marker for reductive dehalogenation. The tree shows sequences from cold seep metagenome-assembled genomes obtained in this

study (blue) alongside representative reference sequences (black). The subgroup of each reference sequence is denoted. The tree was constructed using the JTT matrix-based model, used all sites, and was bootstrapped with 50 replicates and midpoint-rooted.





**Supplementary Figure 14** Depth-differentiated metabolic capacity based on normalized short-read counts of genes encoding the catalytic subunits of key metabolic enzymes in unassembled quality-filtered reads. Genes are marked by different colors. Details on the annotation of the enzymes are presented in **Supplementary Data 5**.



**Supplementary Figure 15** Maximum-likelihood tree of amino acid sequences of catalytic subunits of canonical fumarate-adding enzymes, which are markers for anaerobic hydrocarbon degradation. The tree shows sequences from cold seep metagenome-assembled genomes obtained in this study (blue) alongside representative reference sequences (black). Different clades correspond to alkylsuccinate synthases (AssA), benzylsuccinate synthases (BssA), naphthylmethylsuccinate synthases (NmsA), and hydroxybenzylsuccinate synthases (HbsA). The tree was constructed using the JTT matrix-based model, used all sites, and was bootstrapped with 50 replicates and midpoint-rooted.

## Supplementary references

1. Lombard, V., Golaconda Ramulu, H., Drula, E., Coutinho, P.M. & Henrissat, B. The carbohydrate-active enzymes database (CAZy) in 2013. *Nucleic Acids Res* **42**, D490-495 (2014).
2. Greening, C. et al. Genomic and metagenomic surveys of hydrogenase distribution indicate H<sub>2</sub> is a widely utilised energy source for microbial growth and survival. *ISME J* **10**, 761 (2015).
3. Müller, A.L., Kjeldsen, K.U., Rattei, T., Pester, M. & Loy, A. Phylogenetic and environmental diversity of DsrAB-type dissimilatory (bi)sulfite reductases. *ISME J* **9**, 1152-1165 (2015).
4. Kublik, A. et al. Identification of a multi-protein reductive dehalogenase complex in *Dehalococcoides mccartyi* strain CBDB1 suggests a protein-dependent respiratory electron transport chain obviating quinone involvement. *Environ Microbiol* **18**, 3044-3056 (2016).
5. Søndergaard, D., Pedersen, C.N. & Greening, C. HydDB: A web tool for hydrogenase classification and analysis. *Sci Rep* **6**, 34212 (2016).